Zero waste and biodegradable Zinc Oxide Thin-film Transistors for UV sensors and logic circuits

Gabriel L. Nogueira, Dinesh Kumar, Shoushou Zhang, Neri Alves, and Jeff Kettle

***Abstract*— Bioderived and biodegradable electronics have the capability to reduce significantly Waste Electrical and Electronics Equipment (WEEE) and can also be applied to other sectors where degradation to benign by-products is essential such as marine, farming, or health monitoring. Herein, the authors report biodegradable thin-film transistors (TFTs) arrays based on zinc oxide (ZnO) active layer using molybdenum (Mo) source, drain and gate electrodes. The developed TFTs were fabricated at room temperature onto a planarized biodegradable substrate surface and achieved an Ion/Ioff ratio of ~4×10^6, a threshold voltage of ~2.3 V, field-effect mobility in the saturation region of 1.3 cm^2 V^{-1} s^{-1}, a subthreshold swing of 0.3 V dec^{-1} and show stable device performance under stability tests. Based upon the successful fabrication of the ZnO TFT array, the demonstration of a UV sensor (phototransistors mode) and simple logic circuits (inverter and both NAND and NOR gate circuits) are presented. Further, a method to 'control' the transience was implemented by using a printed heater that could accelerate the decomposition of material, which opens potential avenue for material recovery and zero waste products.**

***Index Terms*— biodegradable electronics, molybdenum, thin-film transistors, zinc oxide.**

I. Introduction

THE desire to reduce the volume and consequential impact of electronic waste (*e*-waste) has brought about a growing interest in electronic devices containing more environmentally friendly materials. For instance, biodegradable electronics devices, that are made from materials that dissolve into benign and biocompatible by-products, provides unique opportunities for applications in new optoelectronic, electronic, and sensing systems.[1] The development of the fully biodegradable electronics requires investigation of alternative substrates, insulators, metals, semiconductors and encapsulation; all of these elements need to provide adequate performance, reliability and degradability for future commercial applications. In terms of substrates, new options have emerged by adopting bio-based materials such as those based on Polylactic acid (PLA), Polyhydroxyalkonoates (PHAs), starch blends, or cellulose based plastics.[3] However, these materials impose additional constraints for electronic processing as they are only suitable for low temperature processing (<150˚C) and have a higher surface roughness than existing electronic substrates. Additional challenges are related to the selection of Ohmic contacts because there is a small sub-group of metals that are known to biodegrade. Commonly used electrode metals include gold (Au), silver (Ag), platinum (Pt), and copper (Cu), but these are not suitable for green electronics because of their non-biodegradable nature, low relative abundance, and pollution they create over their entire cradle-to-grave life cycle.[4] By contrast, magnesium (Mg), Zinc (Zn), Tungsten (W), Iron (Fe), Molybdenum (Mo) have been identified as the main alternative choices, due to their biocompatibility and easy of disposal.[6]

The sourcing of biodegradable semiconductor materials is another pressing issue in order to reduce e-waste.[5] So far, Ultra-Thin Silicon (UTS) has been used to manufacture biodegradable devices, but silicon electronic manufacture is known to be energy intensive from Life Cycle Assessments (LCAs) studies.[8] Other semiconductor materials that are known to be biodegradable include is Zinc Oxide (ZnO), (bandgap ~3.4 eV) which has been widely studied in recent years for flexible electronic and optoelectronic devices.[9], [10] ZnO has already been demonstrated in wearable[11] and, more recently, epidermal or skin-like devices, such as UV-dosimeter temporary tattoos or highly stretchable photodetectors have shown great potential for health monitoring.[12], [13] Nevertheless, there are few reports of entirely biodegradable devices and circuits having been made, especially as the choice of electrode to use in conjunction with ZnO has not been considered.

In this paper, the manufacture of biodegradable ZnO TFT after careful material selection of the electrode, dielectric, and

This work was supported in part by the Coordenação de Aperfeiçoamento de Pessoal de Nível Superior - Brasil (CAPES) - Finance Code 001 and the University of Glasgow's EPSRC IAA grant (EP/R511705/1) and 'GEOPIC' (EP/W019248/1). (*corresponding author: Jeff Kettle*)

J. Kettle is with University of Glasgow, James Watt School of Engineering, Glasgow, Scotland, UK. (e-mail: jeff.kettle@glasgow.ac.uk). G. L. Nogueira and N. Alves are with the São Paulo State University – UNESP, Faculty of Science and Technology (FCT), Physics Department, Presidente Prudente, SP, Brazil. (e-mails: leonardo.nogueira@unesp.br; neri.alves@unesp.br).

D. Kumar and S Zhang are with Bangor University, School of Electronics, Bangor, Gwynedd, Wales, UK.

substrate is reported. To achieve this, Mo electrodes have been used and a detailed discussion about the formation of ohmic contact between Mo/ZnO is also presented in the Section 2. Subsequently, the performance of the low-temperature ZnO TFTs are reported as well as the adaptation for UV photo sensors, and the demonstration of complex logic circuits, which could be used for logic circuits or sensor systems in the future. Finally, degradation studies are conducted.

II. Electrode Selection for Sustainable Electronics Preparation

A. Biodegradable and commonly used electrodes for ZnO TFTs

Considering the range of metals, which are either already used as Ohmic contacts in ZnO TFTs or are known to degrade into benign end-products, a list of potential electrodes options is shown in Fig. 1a by considering the current market costs (euro kg^{-1}) and their global abundances (ppm).[14] Based upon this analysis, the use of Fe as electrodes would be desirable as it provides a best balance of low-cost and high availability. By contrast, Ag has a comparatively higher cost and lower abundancy so is clearly undesirable from a cost and sustainability perspective for ZnO TFTs. In addition, Fig. 1b summarizes the dissolution rates of metals in physiological conditions and in deionized water (DI), where Ag, Ti, and Al were left out of this analysis as they are not considered degradable. Data for the dissolution rate in DI shown in Fig. 1b is also useful in an environmental context. It is clear that all of these metals exhibit fast dissolution rates, although Mo, followed by Fe, appear to be the most resilient, but considering that TFTs typically use electrodes with thickness <100 nm, even the most resilient electrodes would likely degrade within 100 days of exposure to the mediums. As such, encapsulation of final devices will be a prerequisite for many practical applications.

In order to review the impact of electrode material selection in ZnO TFTs, we applied a life cycle impact assessment approach using the USEtox version 2.12 model to determine potential impacts on human health (cancer and non-cancer disease) and ecological toxicity, using a methodology reported by Chen et al[15] and Singh et al[16]. The model outputs the environmental fate, effect parameters, and also improves understanding and management of chemicals in the global environment by further applying the model to describe the exposure and effects of chemicals.

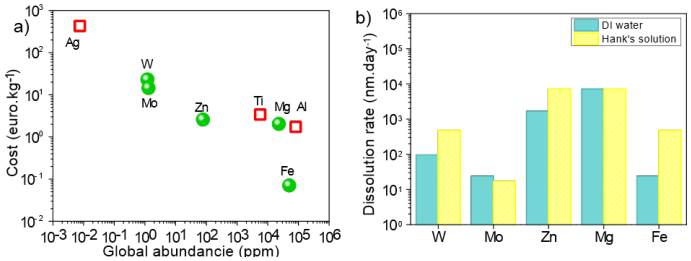

Fig. 1. (a) Map of cost and global abundance values for representative metals for ZnO contacts. The green spheres represent biodegradable metals. (b) Dissolution rates of the principal bioresorbable metals in physiological conditions (Hank's solution, pH 7.4 and 37ºC) and in deionized water (DI).

The results are shown in Fig. 2 and can be used for eco-design of the electrode choices. In this study, we chose the USEtox "mid-point effect" which minimizes inference of data and uncertainties caused by interactions between different impacts. The potential carcinogenic and non-carcinogenic impacts of eco-toxicity and human toxicity of the selected metals were calculated according to the Equation 1:

$$ISx = W.Cfx \quad (1)$$

where, IS_x representing the impact score of metal x in the TFT; W is the total weight of the electrode (in kg); and Cf_x is the characterization factor for the corresponding potential of metal x. The units of the characterization factor for human toxicity and ecotoxicity were cases $(kg_{emitted})^{-1}$, and potentially affected fraction (PAF) of species due to change in concentration of toxic emissions.[17]

In terms of the human toxicity impacts of the metals (Fig. 2a), the rank of best to worst choice is Mo, Zn and finally Ag. Fe and Mg tend to absorbed by the body naturally so are not applicable for human toxicity calculations. In terms of ecotoxicity impacts (Fig. 2b), the rank of best to worst choice is Mo, Fe, Zn, Ag and finally Al. In the case of Ag (on average 3200 PAF m^3 day kg^{-1}), this is primarily due to environmental damage caused in the full life cycle, including such processes as mining, purifying and transportation. It is clear that Mo and Fe show the best characteristics for electrode selection in ZnO TFTs, when considering the cost, abundance, degradability and human and environmental impact (Fig. 2c). However, reports of the use of Mo or Fe electrodes in large area electronic are quite rare [22], possibly because Al and Ag are very simple and effective and eco-design has not been widely considered.

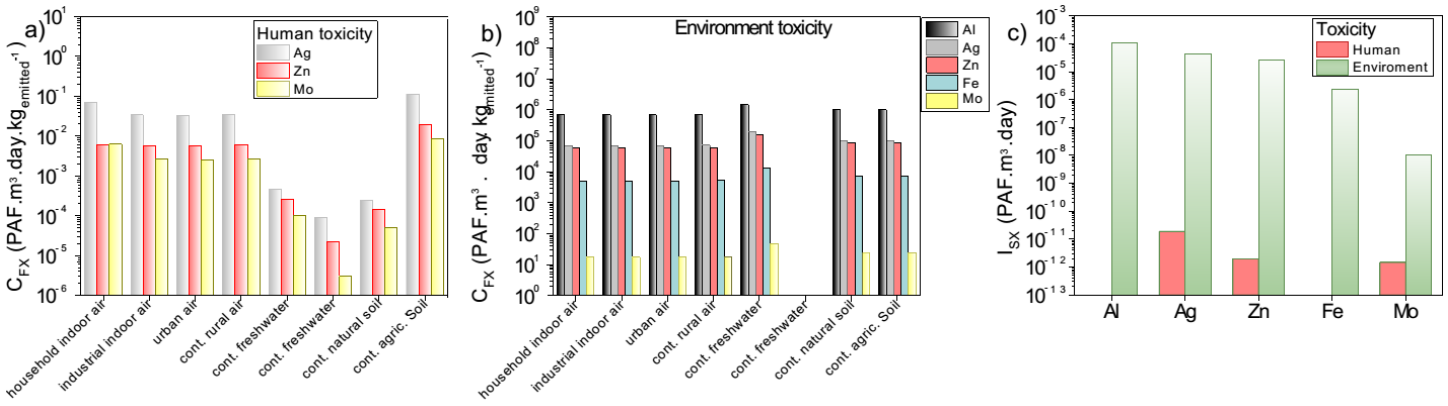

Fig. 2. (a) Midpoint human health characterization factor [cases $kg_{emitted}^{-1}$] non-cancer total human toxicity and (b) Midpoint ecotoxicity characterization factor [PAF m^3 day $kg_{emitted}^{-1}$]. Both scores resulted from the USEtox 2.12 life cycle assessment of representative biodegradable metals. (c) Eco-toxicological impact and the total human toxicity risk result using the metal mass of 100 nm thin films.

B. Suitability of Mo source/drain electrode for ZnO

As a result of the sustainability analysis, Mo and Fe are seen as promising candidate materials for ZnO TFTs, but understanding it's behaviour as ohmic contacts with ZnO is vital.[20] For instance, Ning et al. reported the formation of a molybdenum oxide interlayer between the Mo and a-STO that prevent the diffusion of Mo atoms into a-STO film resulting in a better-quality contact interface[18]. In terms of electrical behaviour, for an ideal metal-semiconductor junction, the barrier height for electron injection (Φ_B) depends primarily on the metal work function (Φ_M) and the electron affinity of the semiconductor (χ_S), and is given by the Mott-Schottky equation:

$$\Phi_B = \Phi_M - \chi_S \quad (2)$$

According to the Equation 2, the formation of an ohmic contact for an n-type semiconductor requires Φ_M to be close to or smaller than χ_S. However, practical devices have long been known to deviate from this ideal behavior.[21] Fig. 3a shows the work function and it is clear that the work function value of Mo electrodes lies in such a range that the formation of an ohmic contact purely in terms of the difference between the Φ_M and ZnO electron affinity is unlikely. The affinity of oxygen to metals is one aspect that can affect the working mechanism of ZnO devices, as shown with Ti electrodes,[27] however the oxygen affinity to Zn is higher than to Mo, so the authors consider this unlikely to lead to Ohmic contact formation either. However, the ohmic contact can also be explained by tunneling through the barrier. In general, tunneling will only be dominant for high doping concentrations.[24] Therefore, the formation of ohmic contact to ZnO can be achieved by increasing the ZnO surface doping density, which narrows the depletion width and increase the probability of electron tunneling. This formation of a metal/ZnO ohmic contact arises as a result of the oxygen vacancies and ensures the working of devices based on the Mo or Fe biodegradable electrodes. The ZnO/Mo ohmic contact formation should be related to the exposition of ZnO surface to the intense impingement that is the sputter process[25] during the Mo top electrodes deposition. For example, Hu et al. reported a superior ZTO ohmic contact formed using sputtered Mo when compared to evaporated Mo.[19] For IGZO and ZTO, sputtering may change chemical states and create a conductive region at the interface or deep in the semiconductor film. The resistivity of oxide semiconductors can be reduced by argon or hydrogen plasma treatment, possibly due to the formation of extra oxygen vacancies or other doping states. For ZnO, it is reported that the ion bombardment during the Ar plasma treatment decreases the contact resistance because of the formation of oxygen vacancies on ZnO surface,[26] which can also enhance the ZnO TFT performance.

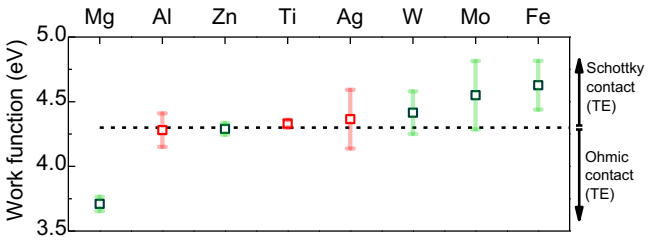

Fig. 3. (a) Average values of work function (eV) for representative metals,[45], [46] in which the green squares represent the biodegradable ones. The dashed line represents the electronic affinity value of ZnO.

III. Experimental Section

A. Substrante development

In this work, Poly(3-hydroxybutyrate-co-3-hydroxyvalerate) (PHBv) was used as the substrate for TFT device fabrication. PHBv is a biodegradable, nontoxic, biocompatible plastic produced naturally by bacteria and undergoes bacterial degradation in the environment. One of the challenges of using PHBv directly in electronics are the low glass transition temperature (T_g ~80 ºC) and low melting point (T_m ~150 ºC), and the relatively high surface roughness [27]. As a result, the processing temperatures had to be kept below 80 ºC. In order to ensure compatibility with the PHBv substrate, planarization was required. A planarization layer is needed as the substrate must have strong adhesive properties, be able to sustain moderate temperatures, be free of impurities that migrate into the active layer and planarize the surface adequately for device fabrication. For TFT fabrication, the surface properties of the substrate are very demanding as the electrodes and semiconductor needs to be deposited onto a low roughness underlying substrate (typically average surface roughness (R_A) <20 nm), otherwise the semiconductor layer will inevitably contain many traps at the dielectric and semiconductor interface. Therefore, polyvinyl acetate (PVAc) was used to planarise the surface prior to device fabrication. PVAc with a typical molecular weight (M_w) of 80,000-100,000 was used, as received from Sigma-Aldrich. PVAc (3 wt%) were spun onto the PHBv substrates at 3000 rpm and annealed at 50°C in air atmosphere for 1 hour. The thickness of the PVAc was measured at 150 nm using profilometry.

B. TFT fabrication and testing

Molybdenum (Mo) metal was sputter coated onto the substrate using a Leybold 350 sputter coater with argon gas. The power density used for the Mo deposition was 1.35 W cm^{-2} and the flow rate of the Ar/O_2 gas was set at 20 sccm at a pressure of 20 mTorr. The deposition rate was measured at 1 Å s^{-1} with a final thickness of 50 nm. Subsequently, an aluminum oxide (Al_2O_3) dielectric layer of 60 nm thick was deposited using Leybold350 Electron-beam evaporator using 1-3mm of clear Al_2O_3 pieces with 99.99% purity. The deposition rate was kept below 2 Å s^{-1} for uniform layer deposition[28]. The optimum thickness for the Al_2O_3 gate-oxide film was measured at 60 nm based upon electrical data. ZnO layers were deposited using radio frequency (RF) sputtering technique. The power density used for the ZnO deposition was 0.95 W cm^{-2} and the flow rate of the Ar/O_2 gas was also set at 20 sccm at a pressure of 20 mTorr. The deposition rate was measured at 0.5 Å s^{-1} with a final thickness of 50 nm. No post annealing of films was applied, but the substrate was cooled during film deposition to avoid overheating of the PHBv substrate. The 99.99% pure ZnO target was pre-sputtered under closed shutter conditions for 5

min to eliminate any surface contaminants. Finally, source and drain Mo electrodes were deposited resulting in an 800 μm and 50 μm channel width and length, respectively (scheme on inset of Fig. 4a). Surface roughness was characterized using mechanical profilometry in order to identify processing anomalies over large areas to be identified, which is necessary for TFT arrays. For the TFT measurements, a two-channel source-measure unit (SMU, Keithley) was used, with probe connectors to perform the contacts to the electrodes (drain, source, and gate) and a voltage sweep ratio of 0.5 V s^{-1} for both V_{DS} and V_{GS}. For UV saturation experiments, the ZnO TFTs were exposed to UV light with wavelength of 355 nm for one minute, with the power measured at an irradiance of 0.20 mW mm^{-2}.

IV. Results

A. ZnO TFT performance

In this work, PVAc was applied to level and minimize the surface roughness of the PHBv. Initially, the surface roughness was reduced from an average surface roughness (R_A) of 530 nm to 55 nm, and the peak-to-valley (R_Z) roughness from 84 nm to 16 nm, i.e., an improvement of ~9.5× and ~5× of R_A and R_Z, respectively. After deposition of gate metal (Mo), the surface roughness did not change significantly either. The Al_2O_3 gate dielectric was obtained by E-beam deposition. Previously, Al_2O_3 thin-films for TFT gate dielectrics are typically deposited from sputtering, anodization, or Atomic Layer Deposition (ALD), but these are difficult to achieve given the chemical susceptibility and low T_g of the biodegradable substrate. Initially, Al_2O_3 metal-insulator-metal (MIM) capacitors were made and then tested using impedance spectroscopy which yield a capacitance per unit area of 2.5×10^7 F cm^{-2}, which compares to around 3.8×10^{-7} F cm^{-2} for sputtering [29] and 1.5×10^{-7} F cm^{-2} for ALD [30]. Electrical characterization of the MIM capacitors show low leakage current between -20V to 20V with a value of 2.5×10^{-10} A/cm^2.

ZnO TFTs were then fabricated and the characterization is presented in Fig. 4 where output (a) and transfer curves (c) are shown. From the plot of output curves, we see that the drain current (I_{DS}) increases as the drain voltage (V_{DS}) is increased from 0 to 10 V. The curves are plotted for different positive gate bias clearly show the device to be operating in the enhancement mode, achieving saturation at high values of V_{DS}. The clear pinch-off and saturation region of the output curves imply that the free electrons of the ZnO channel can be depleted. The source/drain contact's quality of the TFT is better evaluated by depicting the derivative ($\delta I_{DS}/\delta V_{DS}$) of the output curves at low V_{DS} region.[51] For our ZnO-TFT, Fig. 4b shows both the linear drain current behavior and the $\delta I_{DS}/\delta V_{DS}$ curves within the region of V_{DS} from 0 to 2.0 V. The absence of "current crowding" behavior demonstrates moderately good contact between source/drain electrodes (Mo) and the semiconducting channel (ZnO). Then, following the discussion in Section 2, the use of Mo contacts enables a biodegradable TFT to be fabricated and it has a minor impact on device performance when compared to using the more toxic metals such as Al or Ag.

The transfer curve for the device operating in the saturation region is shown on Fig. 4c. Considering the I_{on}/I_{off} ratio as the ratio of the maximum to the minimum I_{DS}, a value of ~4×10^6 was achieved. The $I_{DS}^{1/2}$ *versus* V_{GS} curve is also depicted in Fig. 4c, which allows the evaluation of the threshold voltage (V_{th}) from the extrapolation of the linear region to the horizontal axis and the mobility (μ) from the slope of the curve:

$$I_{DS}^{1/2} = \sqrt{\frac{W}{2L}\mu C_i}(V_{GS} - V_{th}) \quad (3)$$

Considering the C_i mentioned before and the W/L of 16, we extracted values of V_{th} and μ of ~2.3 V and 1.3 cm^2 V^{-1} s^{-1}, respectively. The saturation mobility (μ) can also be calculated from the transconductance with high V_{DS}:

$$\mu_{sat} = \frac{2L}{WC_i}\left(\frac{\partial I_{DS}^{1/2}}{\partial V_{GS}}\right)^2, \quad (4)$$

Where C_i is the gate insulator per unit area, W is the channel width, and L is the channel length. Fig. 4d shows the plotting of μ versus V_{GS} that allows for a more complete understanding of the device behavior than the single peak or mean value of μ.[33] The extracted values of V_{th} and μ are similar to the report of Li et al. and Varma et al. using low temperature ZnO thin films.[31], [34] In total, 28 devices were fabricated and the variation in device performance is shown in Fig. 4e and 4f for V_{th} and μ, respectively. Variability of device performance is largely comparable to performances achieved from sputtered deposition approaches onto glass substrate devices.[35]

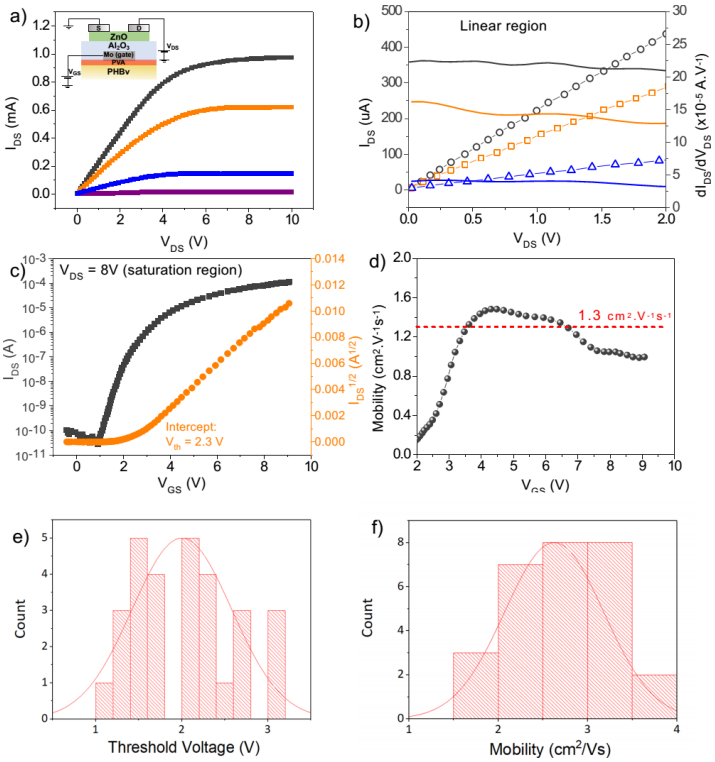

Fig. 4. (a) output curves for different V_{GS} steps. (b) The linear region of the output characteristic and the derivative of I_{DS} vs V_{DS} (solid curves). (c) Transfer curve and $Id^{1/2}$ vs V_{GS} for V_{DS} = 8 V. (d) Mobility dependence of V_{GS}. Histograms showing (e) V_{TH} and (f) μ variation

across 28 identical devices. All plots related to the ZnO TFT with Mo electrodes.

Another important parameter to evaluate the ZnO TFT is the subthreshold swing (SS), which indicates the change in gate voltage required to increase the drain current by one decade in the sub-threshold region ($V_{GS} < V_{th}$). The SS is defined as the inverse of the maximum slope of transfer characteristics:

$$SS = \left(\frac{d\,log(I_{DS})}{dV_{GS}}\right)^{-1} \quad (5)$$

The SS also provides valuable information since it is related to the total trap density (N_t) near the semiconductor/gate dielectric interface, as shown by the Equation 6:[36]

$$N_t = \left(\frac{S\,log\,(e)}{\frac{kT}{q}} - 1\right)\frac{C_i}{q}, \quad (6)$$

Where C_i is the gate insulator capacitance per unit area, k is the Boltzmann constant, and q is the charge of an electron. Based upon the data in Fig. 4c, the calculated values of SS and N_t are 0.3 V dec^{-1} and 6.3×10^{12} cm^2 V^{-1} s^{-1}, respectively. The values reported here are in agreement with the founds of Kandpal et al.[37] and Dong et al.[38].

It is worth noting that the performance of the device is slightly lower than the state-of-the-art in this field. The reason for this is twofold; first, the surface roughness of the dielectric is still relatively higher than conventional substates (typically glass) and could be improved with further optimization and reductions in the surface roughness. Secondly, the ZnO could not be annealed due to the underlying PHBV substate and PVAc layer, which means the device cannot be processed at temperatures greater than 150 ºC. Typically, ZnO films are annealed at temperatures greater than 300 ºC; however, one of the benefits of sputtered films, over ALD or spray deposited ones, is that they seem more tolerable of low temperature processing as grain sizes are larger – typically around 120 nm using our processing route[10].

Considering the TFT architecture with ohmic contact, the output curves were simulated via the COMSOL software. Fig. 5a shows output curves simulated for a ZnO-based TFT with Mo ohmic contacts by using the simplified geometry and dimensions shown on the inset of Fig. 5b. For this simulation, it was used parameters such as μ = 1.5 cm^2 V^{-1} s^{-1} and a doping density (N_d) of 1×10^{23} m^{-3} uniform along with the film thickness. Fig. 5c shows the output curves simulating a condition in which the surface is heavily doped, with a ten-time higher donor concentration than the bulk. Based on the similarity of these curves with the ones shown in Fig. 4a, we note that a moderated increase in the doping density at the surface does not prevent the device from working properly. However, when the surface doping density is increased, it became difficult to reach the expected saturation of I_{DS} at low voltage as found experimentally. Fig. 5d shows the output curves for V_{GS} = 8V simulated for all doping density profiles shown in Fig. 5b. The current normalized by the maximum value of the set curves enables a better shape comparison, and the curves without normalization are shown in the inset presenting the difference in I_{DS} magnitude. The distortion of I_{DS} saturation becomes relevant from a doping density surface a hundred times bigger than bulk density. Once the surface doping density stay below critical values, the simulation results are compatible with the experimental behavior. Thus, it is likely that the existence of a suitable surface doping, as described before, occurs due to a plasma environment during the sputtering procedure of Mo deposition on the ZnO film.

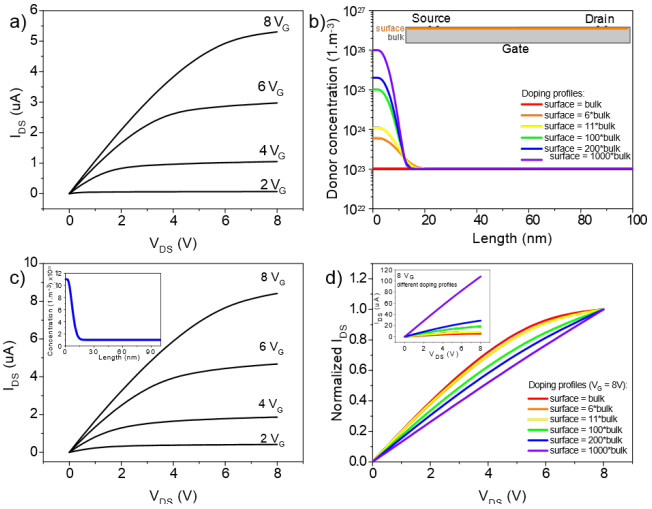

Fig. 5. COMSOL simulation for a ZnO TFT with a Mo source/drain ohmic contacts. (a) Output curves for different V_{GS} steps for a constant donor concentration of 1×10^{23} m^{-3}. (b) A plot of different doping profiles keeping the donor concentration of 1×10^{23} m^{-3} within the semiconductor bulk and increasing the near-surface values. The top-electrodes/semiconductor interface is positioned at zero length. (c) Output curves for different gate bias keeping the donor concentration shape as shown on the inset (11×10^{23} m^{-3} at zero length). (d) Normalized output curves with V_G = 8V for each profile. The inset shows the difference in I_{DS} magnitude at the same V_G = 8.

B. Biodegradable UV sensors

In order to evaluate the optical properties and to the determination of its energy gap, UV-Vis measurement of the sputtered ZnO thin films was conducted (not shown here). ZnO exhibited a high absorbance in the UV region, and a transmittance value of about 99.8 % at the visible light (550 nm). The absorbance 345 nm peak is an important information regarding the UV sensing application of ZnO-TFT. The optical bandgap of the ZnO was determined by applying the well-known Tauc's plot. The coefficient 0.5 is set to the direct transition type of ZnO thin film. Thus, the Tauc plot for direct allowed transitions yields the bandgap calculated value of 3.38 eV and a plot slope of 5.53×10^{14}, which are in good agreement with ZnO thin film values found on literature.[39]

Fig. 6a shows the effect of UV light on the characteristics of the biodegradable ZnO TFT with Mo electrodes. The sensing tests were carried out by monitoring the transfer curve measured in dark and after exposed the device to a UV-355 nm LED for one minute. The UV light changed dramatically the curve, decreasing the I_{ON}/I_{OFF} ratio to around 50 and increasing the I_{ON} by a one order of magnitude. To evaluate the performance of the ZnO TFT as a photodetector, the contrast ratio (sensitivity) was recorded. The contrast ratio is an important figure-of-merit of an UV detector that is defined as the ratio of the light current to the dark current.[40] Fig. 6b shows the dependence of contrast ratio with the gate bias (V_{GS}), in which the highest sensitivity (~10^4 - 10^5) is seen

at V_{GS} range related to the OFF-state of the TFT. In short, such photoconductive effect can be attributed to the generation of the photo excited carriers, which changes the behavior of the ZnO from semiconductor to conductor. Viera et al. [47] and Kumar et al. [41] reported a time-dependent photocurrent for ZnO films, which show a transient recovery response, which limits the phototransistor speed of operation. Even at high doses of UV irradiation (13 W m^{-2}), the electrical performance normally recovers to close to its original value within 30 minutes [47]. The marked increase in the observed response of the ZnO TFT with Mo electrodes under UV light of wavelength 355 nm indicates that our biodegradable device can clearly be used as a UV detector.

Responsivity and EQE of the ZnO TFTs were evaluated by measurement carried out from transfer curve at V_{DS} = 15V at room temperature in air. These properties are given, respectively, by equations (8) and (9):

$$Responsivity = \frac{{}^{I_{total}-I_{dark}}/_{A_{pt}}}{{}^{P}/_{A_{pd}}} = \frac{J_{ph}}{P} \quad (8)$$

$$EQE = \frac{{}^{J_{ph}}/_{q}}{{}^{P}/_{h\nu}} \quad (9)$$

The responsivity and EQE values were calculated at 355 nm wavelength, and were measured are 8.60×10^{3} A W^{-1} and 3.6×10^{3} el ph^{-1}, respectively. This value of responsivity is similar to other reported works of ZnO TFT UV sensors. For example, Kumar et al reported 3.65×10^{4} A W^{-1} and 1.27×10^{5} el ph^{-1}, respectively.[10] Guo, *et al*, manufactured photoconductors based on transistor with mechanically exfoliated single layer of Graphene/ZnO QDs, which displayed responsivity of 10^{4} A W^{-1} at UV wavelength of 325 nm.[42] To our knowledge, this paper reports the best performing biodegradable UV TFT photosensors.

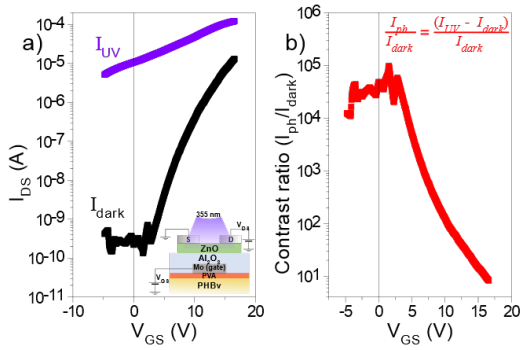

Fig. 6. (a) Transfer curve for the ZnO TFT with Mo electrodes, before and after UV exposure (355 nm) for one minute. (b) Dependence of contrast ratio with the gate bias (VGS).

C. Demonstration of biodegradeable logic circuits

To investigate the potential of the biodegradable ZnO TFT as logic circuits, a simple inverter circuit using a diode-connected TFT load was built by serially connecting a TFT load to the ZnO TFT, as shown on the inset of Fig. 7b. Fig. 7a shows the measured static voltage transfer characteristic for 3, 6, and 9 supply voltages (V_{DD}). The W/L ratios for the driver and load transistors were (2500 µm)/(50 µm) and (625 µm)/(100 µm), respectively. When the input voltage (V_{IN}) of the inverter was low, the driving transistor was in an off-state. Hence, a high output voltage (V_{OUT}) is produced that is the same as the V_{DD}. Alternately, when V_{IN} is high, the transistor is in an on-state. Thus, a low V_{OUT} is transferred as an output. Voltage gain curves that is defined as $V_{gain} = -dV_{OUT}/dV_{IN}$ were plotted for the different V_{DD} bias in Fig. 8b. The inverter showed a sharp response that the maximum V_{gain} is 290 as V_{DD} of 9 V.

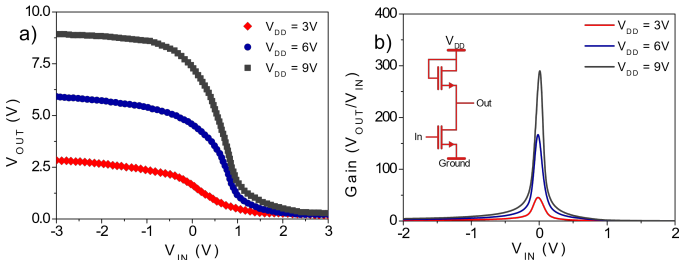

Fig. 7. Measured characteristics of the inverter: (a) Voltage transfer characteristics (VTC) and (b) corresponding voltage gain curves of the inverter for 3, 6, and 9 supply voltages (VDD). Inset: circuit diagram of the diode load inverter.

To further investigate the logic functionalities with the biodegradable ZnO TFT, both NAND and NOR gates were also configured. They were composed of two drivers TFTs connected to a load transistor. A circuit diagram, a truth table, and the measured dynamic output characteristics of the logic gates are exhibited in Fig. 8a and 8b. Here, a high V_{IN} of 12V is defined as '1' and a low V_{IN} of 0 V is defined as '0'. In the NAND logic gate, the output is '1' when both V_A and V_B are '0'. In the NOR logic gate, the output is '0' only when both V_A and V_B are '1'.

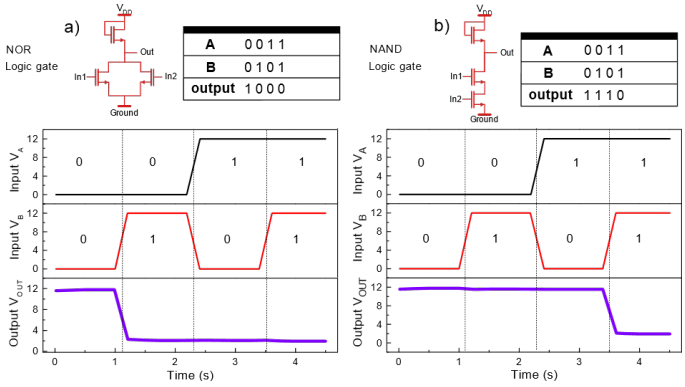

Fig. 8. (a) NOR and (b) NAND logic circuit composed of two ZnO TFT transistors: circuit diagram, truth table, and measured dynamic output characteristics.

D. Biodegradability tests and "controlled" degradation

Previous studies have explored the transient behavior of the biodegradable devices. It is known that the degradation kinetics of the constituent device materials depends on many factors including pH, temperatures, film thickness, bulk and surface morphologies.[43] Shown in Fig. 9a is the stability of the ZnO TFTs stored and tested under ambient conditions. Over 100 hours of testing, the devices show stable operation under ambient conditions with no major change in performance. Previous studies using Mg based electrodes show much poorer device ambient stability, so the benefit of

using the Mo based electrode, as we have done in our work, is evident. Also shown is the behaviour of the developed ZnO TFTs when degraded in a Phosphate-Buffered Saline (PBS) solutions with a pH value of 7.4 and kept at constant temperature (37 °C), which clearly shows rapid degradation in less than an hour as a result of hydrolysis reaction of ZnO and dissolution of Mo.[44]

The results confirm that stable devices are achievable, and that the degradation is strongly dependent on the chemical composition of the surrounding medium and relies on 'passive' or diffusion-driven degradation. As such, we introduce a new method for triggering reactions in transient electronics to achieve 'active transiency'. To accomplish this, a resistive heater was integrated into the underside of the PHBv substrate (see schematic in Fig. 9b). In doing so, elevated heat can be applied to the ZnO TFT arrays, leading to accelerated degradation and, thus, control of the device lifetime. To model the behaviour, an Arrhenius equation was used for modelling and prediction of life at elevated temperatures, as shown in Eq. 10 where the transient life (L) is shown as a function of temperature (T) and where A is a fitting parameters and E_A is the activation energy (eV). For all data fitting in this paper, a 2-point Weibull PDF was used as shown in Eq. 11, where β is defined as the shape parameter, η is the scale parameter, t is the time and f(t) is the probability of failure.

$$L(T) = Ae^{\frac{E_A}{k.T}} \tag{10}$$

$$f(t) = \frac{\beta}{\eta}\left(\frac{t}{\eta}\right)^{\beta-1} e^{-\left(\frac{t}{\eta}\right)^{\beta}} \tag{11}$$

$$A_F = \frac{L_{RT}}{L_{Heater}} = e^{\left(\frac{A}{T_{RT}} - \frac{BA}{T_{Heater}}\right)} \tag{12}$$

Based upon Eq. 10, life as a function of temperature can be plotted on a logarithmic scale to show how varying resistive heater temperature affects the transient behavior of the ZnO TFTs. This is shown in Fig. 9c, with model fittings provided as an inset in Fig. 9d. As can be seen, by increasing temperature, the life of the ZnO TFTs and the degradation follows an Arrhenius relationship with temperature. An important characteristic often assessed in life test models is the acceleration factor (A_F), which shows the ratio of the ZnO TFT lifetime at the room temperature relative to its life at an elevated temperature and is defined in Eq. 12 where T_{RT} and T_{Heater} is room temperature and the heater temperature, respectively, and A is the fitting parameter from Eq 10. For this work, the fitting parameters provide valuable insight into the transient behaviour. As β>1, this indicates that the failure rate (e.g. failures per unit time), increases as time increases. This implies that the failures are driven by 'wear-out' rather than suffering from early life failures. This could be perceived positively as it indicates that the integrated heaters do not stimulate early life failures and that the ZnO TFTs are being driven into 'wear out' mode within a prescribed timeframe. "Active transience" is a new concept proposed in this paper. This approach could be useful for wiping sensitive data from electronic memory devices or providing a method to degrade devices and recover precious metals from electronics. This could open a new paradigm in "Design for Recyclability" applications.

V. Conclusion

There is an increasing demand for electronic technology which are used regularly and on daily basis, but it is vital to meet the net-zero agenda that these are designed without having a negative impact on the environment. We have demonstrated that ZnO TFT arrays can be made using entirely biodegradable

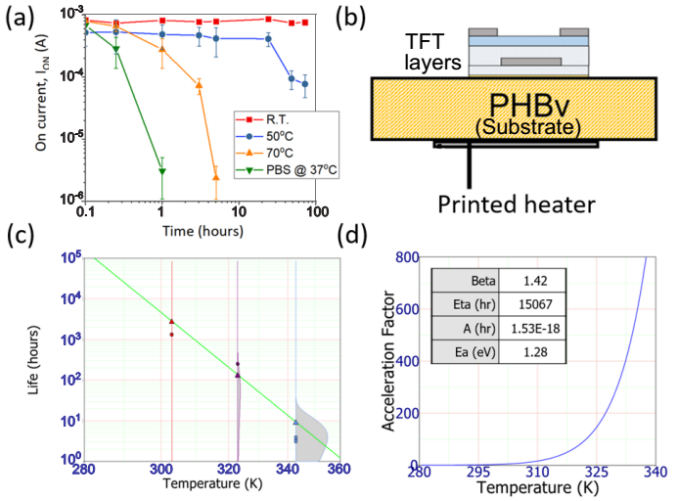

Fig. 9. (a) Electrical stability of the ZnO TFTs tested at room temperature (R.T.), under 50°C and 70°C and in a PBS solution of pH of 7.4 and 37°C. (b) Schematic of a resistive heater integrated into the underside of the PHBv substrate. (c) Transient life, *L(T)*, as a function of temperature in a semi-logarithmic scale, based on Eq. 10. (d) acceleration factor (A_F). inset: fitting parameters of life versus temperature model

materials. The substrate used was PHBv, who surface was modified to reduce the surface roughness by spin coating of a PVAc layer. The gate, drain and source electrodes were deposited by DC sputtering of molybdenum (Mo) film films. Finally, ZnO was selected as the semiconductor layer. As such, all materials used in the work have been proven to be biodegradable from dissolution studies. The TFT performance was quantified and we were able to measure an I_{on}/I_{off} ratio of ~4×10^6, a V_{th} of ~2.3 V and a field-effect mobility (μ) in the saturation region of 1.3 $cm^2 V^{-1} s^{-1}$. After fabrication of devices, applications were demonstrated as UV phototransistors and simple logic circuits. The device achieved a UV sensitivity of ~10^5, the demonstrated inverter achieved a maximum voltage gain of 290 with a supply voltage of 9 V, and both NAND and NOR gate circuits were well operated. We also proposed an active transience approach to achieve a controlled degradation of the device.

Acknowledgment

This study was financed in part by the Coordenação de Aperfeiçoamento de Pessoal de Nível Superior – Brasil (CAPES) – Finance Code 001. We would like to acknowledge the support of the University of Glasgow's EPSRC IAA grant (EP/R511705/1) and the EPSRC grant 'GEOPIC' (EP/W019248/1).

References

[1] X. Yu, W. Shou, B. K. Mahajan, X. Huang, and H. Pan, "Materials, processes, and facile manufacturing for bioresorbable electronics: A review," *Adv. Mater.*, vol. 30, no. 28, p. 1707624, 2018.

[2] L. K. Ncube, A. U. Ude, E. N. Ogunmuyiwa, R. Zulkifli, and I. N.

Beas, "Environmental impact of food packaging materials: A review of contemporary development from conventional plastics to polylactic acid based materials," *Materials (Basel).*, vol. 13, no. 21, p. 4994, 2020.

[3] C. L. Reichert, E. Bugnicourt, M.-B. Coltelli, P. Cinelli, A. Lazzeri, I. Canesi, F. Braca, B. M. Martínez, R. Alonso, and L. Agostinis, "Bio-based packaging: Materials, modifications, industrial applications and sustainability," *Polymers (Basel).*, vol. 12, no. 7, p. 1558, 2020.

[4] W. Li, Q. Liu, Y. Zhang, C. Li, Z. He, W. C. H. Choy, P. J. Low, P. Sonar, and A. K. K. Kyaw, "Biodegradable materials and green processing for green electronics," *Adv. Mater.*, vol. 32, no. 33, p. 2001591, 2020.

[5] F. Witte, "Biodegradable metals," in *Biomaterials Science*, Elsevier, 2020, pp. 271–287.

[6] A. Schauer, C. Redlich, J. Scheibler, G. Poehle, P. Barthel, A. Maennel, V. Adams, T. Weissgaerber, A. Linke, and P. Quadbeck, "Biocompatibility and Degradation Behavior of Molybdenum in an In Vivo Rat Model," *Materials (Basel).*, vol. 14, no. 24, p. 7776, 2021.

[7] R. Li, L. Wang, and L. Yin, "Materials and devices for biodegradable and soft biomedical electronics," *Materials (Basel).*, vol. 11, no. 11, p. 2108, 2018.

[8] N. Krishnan, S. Boyd, A. Somani, S. Raoux, D. Clark, and D. Dornfeld, "A hybrid life cycle inventory of nano-scale semiconductor manufacturing," *Environ. Sci. Technol.*, vol. 42, no. 8, pp. 3069–3075, 2008.

[9] G. L. Nogueira, D. H. Vieira, R. M. Morais, J. P. M. Serbena, K. F. Seidel, and N. Alves, "A Sub-1 V, Electrolyte-Gated Vertical Field Effect Transistor Based on ZnO/AgNW Schottky Contact," *IEEE Electron Device Lett.*, vol. 42, no. 12, pp. 1790–1793, 2021.

[10] D. Kumar, T. C. Gomes, N. Alves, L. Fugikawa-Santos, G. C. Smith, and J. Kettle, "UV phototransistors based upon spray coated and sputter deposited ZnO TFTs," *IEEE Sens. J.*, 2020.

[11] V.-T. Tran, Y. Wei, H. Yang, Z. Zhan, and H. Du, "All-inkjet-printed flexible ZnO micro photodetector for a wearable UV monitoring device," *Nanotechnology*, vol. 28, no. 9, p. 95204, 2017.

[12] Y. Liu, M. Pharr, and G. A. Salvatore, "Lab-on-skin: a review of flexible and stretchable electronics for wearable health monitoring," *ACS Nano*, vol. 11, no. 10, pp. 9614–9635, 2017.

[13] S. Knobelspies, A. Daus, G. Cantarella, L. Petti, N. Münzenrieder, G. Tröster, and G. A. Salvatore, "Flexible a-IGZO Phototransistor for Instantaneous and Cumulative UV-Exposure Monitoring for Skin Health," *Adv. Electron. Mater.*, vol. 2, no. 10, p. 1600273, 2016.

[14] S. R. Taylor, "Abundance of chemical elements in the continental crust: a new table," *Geochim. Cosmochim. Acta*, vol. 28, no. 8, pp. 1273–1285, 1964.

[15] Y. Chen, M. Chen, Y. Li, B. Wang, S. Chen, and Z. Xu, "Impact of technological innovation and regulation development on e-waste toxicity: a case study of waste mobile phones," *Sci. Rep.*, vol. 8, no. 1, pp. 1–9, 2018.

[16] N. Singh, H. Duan, O. A. Ogunseitan, J. Li, and Y. Tang, "Toxicity trends in E-Waste: A comparative analysis of metals in discarded mobile phones," *J. Hazard. Mater.*, vol. 380, p. 120898, 2019.

[17] "EF3.0 Ecotox Explorer." [Online]. Available: https://web.jrc.ec.europa.eu/rapps/pub/ecotox/. [Accessed: 08-Jul-2022].

[18] H. Ning, X. Liu, H. Xu, K. Lu, H. Zhang, X. Zhang, R. Yao, Z. Fang, X. Wang, and J. Peng, "A study of contact properties between molybdenum and amorphous silicon tin oxide thin film transistors," *J. Soc. Inf. Disp.*, vol. 26, no. 12, pp. 681–686, 2018.

[19] W. Hu and R. L. Peterson, "Molybdenum as a contact material in zinc tin oxide thin film transistors," *Appl. Phys. Lett.*, vol. 104, no. 19, p. 192105, 2014.

[20] A. O. M. Alzahrani, M. S. Abdel-wahab, M. Alayash, and M. S. Aida, "Metals and ITO Contact Nature on ZnO and NiO Thin Films," *Brazilian J. Phys.*, vol. 51, no. 4, pp. 1159–1165, 2021.

[21] J. Semple, S. Rossbauer, and T. D. Anthopoulos, "Analysis of Schottky contact formation in coplanar Au/ZnO/Al nanogap radio frequency diodes processed from solution at low temperature," *ACS Appl. Mater. Interfaces*, vol. 8, no. 35, pp. 23167–23174, 2016.

[22] L. J. Brillson and Y. Lu, "ZnO Schottky barriers and Ohmic contacts," *J. Appl. Phys.*, vol. 109, no. 12, 2011.

[23] A. M. Rana, T. Akbar, M. Ismail, E. Ahmad, F. Hussain, I. Talib, M. Imran, K. Mehmood, K. Iqbal, and M. Y. Nadeem, "Endurance and cycle-to-cycle uniformity improvement in tri-layered CeO2/Ti/CeO2 resistive switching devices by changing top electrode material," *Sci. Rep.*, vol. 7, no. 1, pp. 1–15, 2017.

[24] Y. Lv and L. Wan, "Recent progress of ohmic contact on ZnO," in *2008 International Conference on Electronic Packaging Technology & High Density Packaging*, 2008, pp. 1–4.

[25] M. S. Aida, "Energy distribution of Ar ions at the substrate in the sputtering deposition of a-Si: H films," *J. Non. Cryst. Solids*, vol. 160, no. 1–2, pp. 99–104, 1993.

[26] J.-M. Lee, K.-K. Kim, S.-J. Park, and W.-K. Choi, "Low-resistance and nonalloyed ohmic contacts to plasma treated ZnO," *Appl. Phys. Lett.*, vol. 78, no. 24, pp. 3842–3844, 2001.

[27] S. P. C. Gonçalves, M. Strauss, and D. S. T. Martinez, "The positive fate of biochar addition to soil in the degradation of PHBV-silver nanoparticle composites," *Environ. Sci. Technol.*, vol. 52, no. 23, pp. 13845–13853, 2018.

[28] D. Kumar, A. Abdou, and J. Kettle, "Half-volt IGZO flexible thin-film transistors with E-beam deposited Al 2 O 3 gate dielectric," in *2019 IEEE International Conference on Flexible and Printable Sensors and Systems (FLEPS)*, 2019, pp. 1–3.

[29] Z. Jiahui, C. Hudong, L. Honggang, L. Guiming, X. Wenjun, L. Qi, L. Simin, H. Zhiyi, and L. Haiou, "MIM capacitors with various Al 2 O 3 thicknesses for GaAs RFIC application," *J. Semicond.*, vol. 36, no. 5, p. 54004, 2015.

[30] J. Yota, H. Shen, and R. Ramanathan, "Characterization of atomic layer deposition HfO2, Al2O3, and plasma-enhanced chemical vapor deposition Si3N4 as metal–insulator–metal capacitor dielectric for GaAs HBT technology," *J. Vac. Sci. Technol. A Vacuum, Surfaces, Film.*, vol. 31, no. 1, p. 01A134, 2013.

[31] H. Li, D. Han, Z. Yi, J. Dong, S. Zhang, X. Zhang, and Y. Wang, "High-performance ZnO thin-film transistors prepared by atomic layer deposition," *IEEE Trans. Electron Devices*, vol. 66, no. 7, pp. 2965–2970, 2019.

[32] C. Zhao, T.-C. Fung, and J. Kanicki, "Half-Corbino short-channel amorphous In–Ga–Zn–O thin-film transistors with a-SiOx or a-SiOx/a-SiNx passivation layers," *Solid. State. Electron.*, vol. 120, pp. 25–31, 2016.

[33] E. Fortunato, P. Barquinha, and R. Martins, "Oxide semiconductor thin-film transistors: a review of recent advances," *Adv. Mater.*, vol. 24, no. 22, pp. 2945–2986, 2012.

[34] T. Varma, C. Periasamy, and D. Boolchandani, "Performance evaluation of bottom gate ZnO based thin film transistors with different W/L ratios for UV sensing," *Superlattices Microstruct.*, vol. 114, pp. 284–295, 2018.

[35] T. C. Gomes, D. Kumar, L. Fugikawa-Santos, N. Alves, and J. Kettle, "Optimization of the anodization processing for aluminum oxide gate dielectrics in ZnO thin film transistors by multivariate analysis," *ACS Comb. Sci.*, vol. 21, no. 5, pp. 370–379, 2019.

[36] J. S. Park, W.-J. Maeng, H.-S. Kim, and J.-S. Park, "Review of recent developments in amorphous oxide semiconductor thin-film transistor devices," *Thin Solid Films*, vol. 520, no. 6, pp. 1679–1693, 2012.

[37] K. Kandpal, N. Gupta, J. Singh, and C. Shekhar, "Study of ZnO/BST interface for thin-film transistor (TFT) applications," *Surfaces and Interfaces*, vol. 23, p. 100996, 2021.

[38] J. Dong, D. Han, H. Li, W. Yu, S. Zhang, X. Zhang, and Y. Wang, "Effect of Al doping on performance of ZnO thin film transistors," *Appl. Surf. Sci.*, vol. 433, pp. 836–839, 2018.

[39] J. B. Coulter and D. P. Birnie III, "Assessing Tauc plot slope quantification: ZnO thin films as a model system," *Phys. status solidi*, vol. 255, no. 3, p. 1700393, 2018.

[40] A. A. Hadi, B. A. Badr, R. O. Mahdi, and K. S. Khashan, "Rapid laser fabrication of Nickel oxide nanoparticles for UV detector," *Optik (Stuttg).*, vol. 219, p. 165019, 2020.

[41] D. Kumar, T. Gomes, N. Alves, and J. Kettle, "Understanding UV sensor performance in ZnO TFTs through the application of multivariate analysis," in *2018 Ieee Sensors*, 2018, pp. 1–5.

[42] W. Guo, S. Xu, Z. Wu, N. Wang, M. M. T. Loy, and S. Du, "Oxygen-Assisted Charge Transfer Between ZnO Quantum Dots and Graphene," *Small*, vol. 9, no. 18, pp. 3031–3036, 2013.

[43] L. Yin, H. Cheng, S. Mao, R. Haasch, Y. Liu, X. Xie, S. Hwang, H. Jain, S. Kang, and Y. Su, "Dissolvable metals for transient

electronics," *Adv. Funct. Mater.*, vol. 24, no. 5, pp. 645–658, 2014.
[44] A. A. La Mattina, S. Mariani, and G. Barillaro, "Bioresorbable materials on the rise: from electronic components and physical sensors to in vivo monitoring systems," *Adv. Sci.*, vol. 7, no. 4, p. 1902872, 2020.
[45] S. Halas and T. Durakiewicz, "Work functions of elements expressed in terms of the Fermi energy and the density of free electrons," *J. Phys. Condens. Matter*, vol. 10, no. 48, p. 10815, 1998.
[46] H. B. Michaelson, "The work function of the elements and its periodicity," *J. Appl. Phys.*, vol. 48, no. 11, pp. 4729–4733, 1977.
[47] Vieira, D. H., da Silva Ozório, M., Nogueira, G. L., Fugikawa-Santos, L., & Alves, N., "UV-photocurrent response of zinc oxide based devices: Application to ZnO/PEDOT: PSS hydrid Schottky diodes, " Mater. Sci. Semicond., vol. 121. p. 105339, 2021.